Earth and Planetary Science Letters 325–326 (2012) 116–125

Contents lists available at SciVerse ScienceDirect

Earth and Planetary Science Letters

journal homepage: www.elsevier.com/locate/epsl

Ventilation of the deep ocean constrained with tracer observations and implications for radiocarbon estimates of ideal mean age

S. Khatiwala [a,*], F. Primeau [b], M. Holzer [c,d]

[a] Lamont–Doherty Earth Observatory, Columbia University, Palisades, NY 10964, USA
[b] Department of Earth System Science, University of California, Irvine, CA, USA
[c] School of Mathematics and Statistics, University of New South Wales, Sydney, NSW 2052, Australia
[d] Department of Applied Physics and Applied Mathematics, Columbia University, New York, NY, USA

ARTICLE INFO

Article history:
Received 31 May 2011
Received in revised form 12 January 2012
Accepted 31 January 2012
Available online 28 February 2012

Editor: G. Henderson

Keywords:
ocean ventilation
tracers
ideal mean age
radiocarbon age
Green function
inverse modeling

ABSTRACT

Ocean ventilation is the process that transports water and climatically important trace gases such as carbon dioxide from the surface mixed layer into the ocean interior. Quantifying the dominant source regions and time scales remains a major challenge in oceanography. A mathematically rigorous approach, that accounts for the multiplicity of transport pathways and transit times characteristic of an eddy-diffusive flow such as the ocean, is to quantify ventilation in terms of a probability distribution that partitions fluid parcels according to the time and location of their last surface contact. Here, we use globally gridded radiocarbon data in combination with other transient (CFCs) and hydrographic (temperature, salinity, phosphate, and oxygen) tracer data to estimate the joint distribution of age and surface origin of deep ocean waters. Our results show that ~40% and 26% of the global ocean was last in contact with the Southern Ocean and North Atlantic, respectively. Some 80% of the global deep ocean below 1500 m is ventilated from these high latitude regions. However, contrary to the classical description of the deep ocean as a roughly equal mixture of "northern" and "southern" source waters, we find a significantly higher contribution from the Southern Ocean relative to the North Atlantic. We estimate the mean transit time from the surface to the deep North Pacific at 1360 ± 350 y, intermediate between two widely used radiocarbon-based estimates. To reconcile our estimate of the ideal mean age with ventilation age estimates based on radiocarbon, we apply the estimated distribution function to construct a 3-dimensional distribution of the water mass fraction-weighted surface "initial" radiocarbon concentration that can serve as an accurate reservoir age. Radiocarbon ages corrected for this initial reservoir age are found to be in good agreement (within 5%) with our ideal age estimate, demonstrating that it is essential to take into account the spatially variable surface radiocarbon field when computing ventilation ages using radiocarbon. A wide spectrum of ages contributes to the mean age, providing evidence for the fundamentally eddy-diffusive nature of the large-scale general circulation of the ocean.

1. Introduction

Ocean ventilation is the process that transports water from the surface mixed layer into the ocean interior. Understanding this fundamental aspect of the climate system, in particular quantifying where waters sink and how long on average they have remained isolated from the atmosphere, remains a major challenge in oceanography. It has implications in a variety of areas, ranging from the uptake of heat and anthropogenic CO_2, to interpretation of tracer observations, and reconstructing past variations in ocean circulation from paleoceanographic proxies recorded in marine sediments.

In this paper, we address the question of where waters sink and for how long they have been isolated from the atmosphere. While these two aspects are intricately linked, they have generally been treated as separate problems. Classical water mass analysis has long used hydrographic and other quasi-conservative tracers to decompose waters into constituent water masses (e.g., De Brauwere et al., 2007; Johnson, 2008; Tomczak, 1981; Tomczak and Large, 1989). Typically, only a small number of "end members" have been considered, although a more recent variant by Gebbie and Huybers (2010), allows for a much larger number of sources (in their approach any surface point is a potential source). On the other hand, the question of time scales has been addressed through the use of tracers such as chlorofluorocarbons (CFCs) and radiocarbon to yield some measure of the "age" of the water. However, such tracer ages are not an intrinsic property of the flow but weighted transit times that vary from tracer to tracer (Holzer and Hall, 2000; Khatiwala et al., 2001; Wunsch and Heimbach, 2008).

A fundamental difficulty with the traditional approaches described above is that in an advective–diffusive flow such as the ocean, there is no unique pathway or time scale by which a water parcel reaches any interior location. Instead, it is more appropriate to describe a water parcel in terms of a continuous distribution that partitions it according

* Corresponding author.
E-mail addresses: spk@ldeo.columbia.edu (S. Khatiwala), fprimeau@uci.edu (F. Primeau), hm2220@columbia.edu (M. Holzer).

0012-821X/$ – see front matter © 2012 Elsevier B.V. All rights reserved.
doi:10.1016/j.epsl.2012.01.038

to the time and place of last surface contact. Mathematically, this joint distribution is a type of Green function, known in the present context as a "boundary propagator" (BP). While previous studies have simulated BPs and other age tracers in ocean models (England, 1995; Khatiwala et al., 2001; Peacock and Maltrud, 2006; Primeau, 2005), the solutions may be sensitive to model resolution (Peacock and Maltrud, 2006) and parameterization of sub-grid scale processes (England, 1995), thus limiting their applicability. The recent development of a new mathematical inverse technique (Holzer et al., 2010; Khatiwala et al., 2009) based on the maximum entropy approach (Tarantola, 2005) has, however, made it possible to estimate the ocean's boundary propagator directly from observations. This method was previously applied by Khatiwala et al. (2009) to reconstruct the history of anthropogenic CO_2 in the ocean over the industrial period, which required point-wise estimates of the boundary propagator throughout the global ocean. It has also been used by Holzer et al. (2010) to estimate the joint distribution of transit time and surface origin from cruise bottle data in the North Atlantic. Here, we apply data-constrained estimates of the ocean's boundary propagator made by Khatiwala et al. (2009) to provide the first quantitative description of the joint distribution of the age and surface origin of ocean waters for the global ocean. We will focus on the deep ocean, and the various source regions and time scales with which waters in the deep Pacific are ventilated. We also explore the implications of our results for estimates of age based on radiocarbon (^{14}C), a widely used tracer in both modern and paleoceanography.

2. Methods

We start by reviewing some basic aspects of the Green function framework, and then describe the inverse method.

2.1. Green functions, boundary propagators, and transit-time distributions

The boundary propagator (Holzer and Hall, 2000) provides a complete mathematical solution to the problem of partitioning each water parcel according to its time and location of last surface contact. The BP, $\mathcal{G}$, is a type of Green function, i.e., a solution to the advection–diffusion equation for the ocean with an impulse (in time and space) boundary condition (BC) for concentration in the mixed layer of the ocean. It is important to note that $\mathcal{G}$, is an intrinsic property of the ocean circulation and not of any particular tracer. This allows us to write the concentration of any conservative or passive radioactive tracer in the ocean as a convolution between $\mathcal{G}$and the history of that tracer in the surface mixed layer of the ocean,

$$C(\mathbf{x},t)=\int_{\text{surface}} d^2x' \int_{-\infty}^{t} dt' e^{-\lambda(t-t')} C^s\left(\mathbf{x}',t'\right)\mathcal{G}(\mathbf{x},t|\mathbf{x}',t'), \tag{1}$$

where C is the tracer concentration at location $\mathbf{x}$ and time t, C^s is its surface history, and λ is the radioactive decay rate (if any) for the tracer. $\mathcal{G}(\mathbf{x},t|\mathbf{x}',t')d^2x'dt'$ can be interpreted as the fraction of water at $\mathbf{x}$ and t in the ocean interior that was last in contact with the surface patch d^2x' centered around $\mathbf{x}'$ and between time t' and $t'+dt'$. It is this joint distribution $\mathcal{G}$ that we are interested in estimating from tracer data.

2.2. Estimating $\mathcal{G}$ from observations

The mathematical inverse technique used to estimate $\mathcal{G}$ from tracer observations has been extensively discussed by Khatiwala et al. (2009) (hereafter KPH09) and Holzer et al. (2010) (hereafter HPSK10), and only a brief description is given here. The inverse method exploits the fact that Eq. (1) applies to any passive conservative tracer. Multiple tracer observations thus provide a set of constraints from which we can deconvolve $\mathcal{G}$. This deconvolution problem is highly under-determined. To regularize it, a maximum entropy approach (Tarantola, 2005) is used, which is well suited to problems with positive kernels. To further reduce the indeterminancy, the circulation is assumed to be stationary and the boundary propagator $\mathcal{G}(\mathbf{x},t|\mathbf{x}',t')$is estimated for a discrete set of surface patches, i, rather than for every surface point x'. Thus, $\mathcal{G}(\mathbf{x},t|\mathbf{x}',t')\rightarrow\mathcal{G}(\mathbf{x}|\xi,i)$, where $\xi=t-t'$ is the time elapsed since a fluid element at $\mathbf{x}$ was last at surface patch i. In the maximum entropy method, we maximize an entropy functional $S[\mathcal{G}]=-\sum_i\int d\xi\mathcal{G}(\mathbf{x}|\xi,i)log\frac{\mathcal{G}(\mathbf{x}|\xi,i)}{\mathcal{M}(\mathbf{x}|\xi,i)}$ subject to the discretized tracer constraints. $\mathcal{M}$ is a prior estimate of $\mathcal{G}$ which KPH09 take to be an analytical solution to the 1-d advection–diffusion equation known as the inverse Gaussian (IG) (e.g., Waugh et al., 2004). The resulting constrained optimization problem is solved using the method of Lagrangian multipliers. We emphasize that the inverse Gaussian, which is parameterized by a mean and width, only enters the inversion as a prior. Thus, the mean and width parameters of the IG are specified a priori and not subsequently changed (or "fit" to the data). Moreover, the results are not sensitive to the choice of prior, with a uniform distribution prior giving similar results (Holzer et al., 2010).

In their deconvolution, KPH09 used gridded fields of CFC-11, CFC-12, and natural ^{14}C from the GLODAP database (Key et al., 2004), and potential temperature, salinity, oxygen and phosphate from the World Ocean Atlas (2005) (Antonov et al., 2006; Garcia et al., 2006a,b; Locarnini et al., 2006) (WOA05). Oxygen and phosphate were combined into a conservative tracer (Broecker et al., 1998) $PO_4^*\equiv PO_4+O_2/175$. Together, the GLODAP and WOA05 databases provide six constraints from which they estimate $\mathcal{G}(\mathbf{x}|\xi,i)$with respect to 26 surface patches ($i=1,\ldots,26$) selected according to sea surface density (Fig. 1). In KPH09, the focus was on anthropogenic carbon. Here, we apply these estimates of $\mathcal{G}$ to quantify the ventilation of the deep ocean.

We note that the use of observations to constrain ocean circulation has a long history in oceanography (e.g., DeVries and Primeau, 2011; Memery and Wunsch, 1990; Schlitzer, 1993; Stammer et al., 2004; Wunsch, 1984; Wunsch and Heimbach, 2007). In contrast to these previous studies, which typically attempt to estimate the flow field, our approach may be viewed as an attempt to directly constrain the solution (the Green function) to a passive tracer transported by this flow.

3. Results

The data-constrained $\mathcal{G}(\mathbf{x}|\xi,i)$is the joint distribution of the time ξ since, and surface patch i with which, a water parcel at $\mathbf{x}$ was last in the mixed layer. We start by presenting our estimates of the volumetric contribution made by various source regions.

3.1. Source fractions

To estimate the surface origin of interior waters, we calculate the fraction of water, $f_i(\mathbf{x})$, at location $\mathbf{x}$ that originated from patch i regardless of transit time. This fraction is obtained by integrating $\mathcal{G}(\mathbf{x}|\xi,i)$over all time:

$$f_i(\mathbf{x})=\int_0^\infty d\xi\mathcal{G}(\mathbf{x}|\xi,i). \tag{2}$$

Note that the BPs are normalized such that $\sum_{i=1}^{26} f_i(\mathbf{x})=1$. Many of the patches make negligible contributions for a given interior location $\mathbf{x}$. For brevity, we therefore focus on a few key surface regions formed by combining a subset of the 26 patches (see Fig. 1 and its caption): (1) the North Atlantic north of 40°N (NA); (2) the Southern Ocean south of 50°S (ANT); (3) the Southern Ocean between 40° and 50°S (SUBANT); (4) the tropics between 30°S and 30°N (TROP); (5) the subtropics between 30° and 40°N/S (STROP); and (6) the North Pacific north of 40°N (NPAC).

Fig. 2 (left column) shows the distribution of f for NA, ANT, and SUBANT, averaged from 1500 m to the bottom, while the second through fourth columns are the corresponding zonally-averaged sections for the Atlantic, Pacific, and global ocean, respectively. As expected, f_{NA}

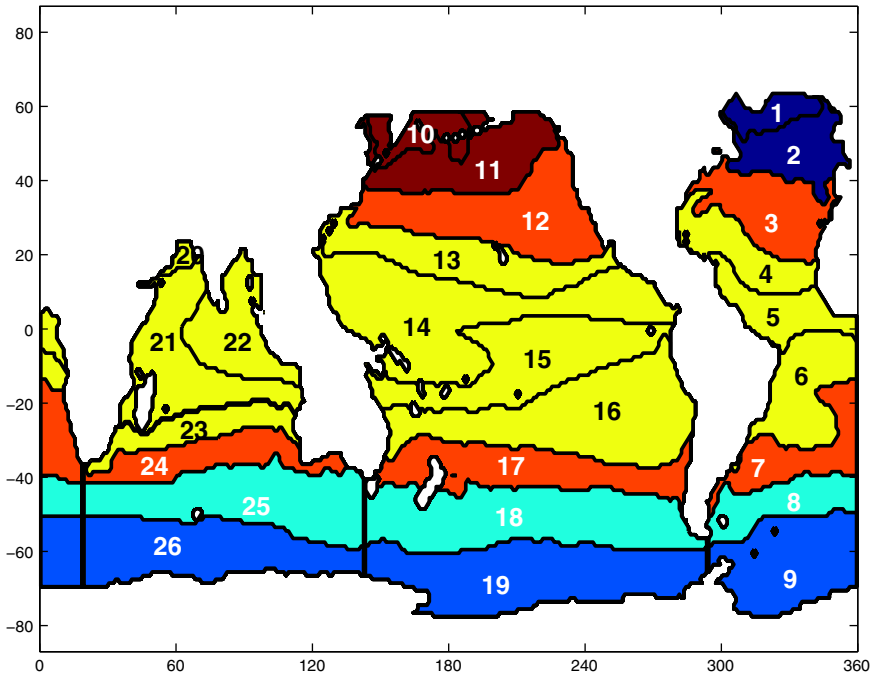

Fig. 1. Surface patches used in the inversion. Black lines and numbers delineate the 26 patches for which $\mathcal{G}$ is estimated, and colors the 6 larger regions discussed in the text: (1) NA: $i=1,2$; (2) ANT: $i=9,19,26$; (3) SUBANT: $i=8,18,25$; (4) TROP: $i=4$–$6,13$–$16,20$–23; (5) STROP: $i=3,7,12,17,24$; and (6) NPAC: $i=10,11$.

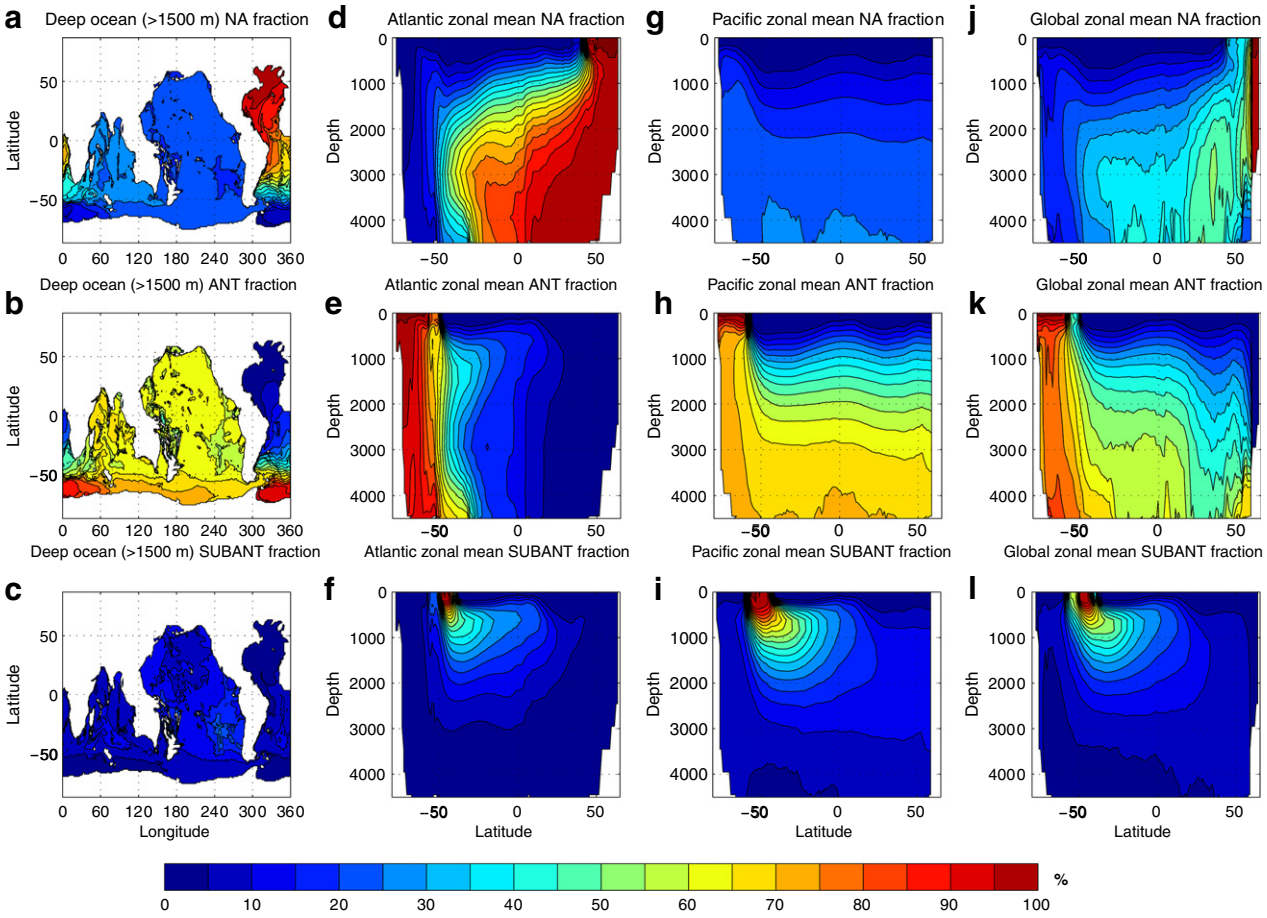

Fig. 2. Water mass fractions (%) for NA, ANT, and SUBANT. Top to bottom: f_{NA}, f_{ANT}, and f_{SUBANT}. Left to right: Depth-weighted average from 1500 m to bottom; zonally-averaged sections for Atlantic, Pacific, and global ocean, respectively.

has its highest values in the North Atlantic, decreasing "downstream" along the path of the "conveyor belt" (Broecker, 1991), or more accurately, the "diffusive conveyor" (Holzer and Primeau, 2006, 2008). f_{NA} is remarkably homogeneous in the deep Pacific, ranging from 0.2 to 0.3. In contrast, both f_{ANT} and f_{SUBANT} decrease away from the Southern Ocean. The deep and bottom waters of the Pacific are dominated by ANT, with f_{ANT} between 0.6 and 0.75. The SUBANT fraction representing Antarctic Intermediate Water is found at a much shallower depth of ~1000 m in both basins.

The point-wise fractions described above are subject to considerable uncertainty. As discussed in more detail by HPSK10, these are largely due to the underdetermined nature of the problem, the so-called "entropic uncertainty". The maximum entropy method allows us to assign a probability density function $p(D)$ for any diagnostic D (such as the fraction f_i) of the $\mathcal{G}$ in terms of the entropy $S[D]$. Computing $S(D)$ (and thence $p(D)$) for a given value of D requires solving a small system of nonlinear equations. Thus, tracing out $p(D)$ for a range of values of D for every grid point is prohibitively expensive computationally. Following HPSK10, we therefore compute $S[D]$ at only a small number of values and fit a power law distribution to S.

There are also errors arising from the sparse spatial and temporal sampling of the various tracers used in the inversion. For instance, as noted by Holzer et al. (2010), convectively driven ventilation, which tends to occur in winter and late spring, may introduce an annual cycle in tracers such as CFCs (e.g. Haine and Richards, 1995; Stommel, 1979; Williams et al., 1995). Ignoring this seasonality, as we do here because of a lack of data, may lead to uncertainty in the surface boundary condition for such tracers. We do account for uncertainty due to mapping errors and choice of prior M by a Monte Carlo procedure (see KPH09) in which the calculation of $\mathcal{G}$ was repeated by randomly sampling the various parameters used in the inversion from a uniform distribution centered about its observed value with a width equal to the reported uncertainty.

Lastly, our approach assumes a steady state ocean circulation. Constraining variability in ocean circulation is a challenging task, and neglecting it will introduce errors in our various estimates. These errors are, however, difficult to quantify (but may be smaller than the intrinsic uncertainty of the method).

Carrying out the above analysis shows that the relative error in point-wise estimates of the fraction $f_i(\mathbf{x})$ ranges from 5% to 50%. These large uncertainties are not surprising given the underdetermined nature of the problem, but can be reduced significantly by averaging $f_i(\mathbf{x})$ over large volumes, as follows: A volume-weighted average of $f_i(\mathbf{x})$ over any given volume yields the fractional contribution of patch i to that part of the ocean. Tables 1–3 list these for the 6 surface regions defined above for the global ocean, Atlantic Ocean, and Pacific Ocean, respectively. In each table, fractional contributions are given for the entire water column, the deep ocean (defined as depths below 1500 m), and select depth intervals. For the global ocean, the Southern Ocean south of 50°S is by far the largest source; roughly 40% of the world ocean was last in contact with this region. The North Atlantic is the next largest source, followed by the Subantarctic. ANT and SUBANT, combined, make up almost 60% of the ocean. Uncertainty estimates of these fractions are typically ±10% of the quoted value.

Both our point-wise and globally integrated source fractions agree well with the estimates of Johnson (2008) and Gebbie and Huybers (2010) (hereafter GH). For example, GH, using a water mass decomposition approach that did not consider the temporal aspect, obtain source fractions for the global ocean of 25% for NA, 36% for ANT, 20% for SUBANT, 12% for TROP + STROP, and 2% for NPAC. (Note that GH use slightly different surface regions than the ones used in our study.) Also in agreement are the estimated spatial variations within each of these regions. For ANT, we find contributions of 23%, 12%, and 4% from the Atlantic, Pacific, and Indian Ocean sectors, respectively. The corresponding values for GH are 21%, 14%, and 1%.

For the deep ocean, however, our results differ significantly from previous work. Specifically, we find that over 80% of the ocean below 1500 m is ventilated from NA and SO, broadly consistent with the classical two end-member description of the deep ocean (Broecker et al., 1998). In contrast to the work of Broecker et al. (1998), which held that the northern and southern end members contribute equally, we find a significantly higher contribution from the Southern Ocean relative to the North Atlantic, 48% and 33%, respectively. It is important to appreciate that Broecker et al.'s analysis was in a number of ways much less complete than ours. For example, they assume only two source regions for the deep ocean and discriminate between them based entirely on PO_4^*. They also use a much sparser dataset, and use a single PO_4^* value of 1.95 μmol kg^{-1} for the Southern Ocean end member. As they point out, if values less than this exist in the Southern Ocean, it would increase the contribution of that region relative to the North Atlantic. Lastly, we note that the assumption that PO_4^* is a conserved tracer is not strictly valid in oxygen minimum zones (OMZs) where denitrification allows for the remineralization of phosphorus without any drawdown in the concentration of oxygen (e.g., Anderson and Sarmiento, 1995). As a result, PO_4^* values downstream of OMZs in the Arabian Sea and Eastern Tropical Pacific are probably slightly higher than they would be if PO_4^* was perfectly conserved. While the effect is small on global scales, the needed correction would further emphasize the importance of the Southern Ocean as the dominant source of deep waters.

Table 1
Global ocean volumetric fractions (%) for different surface source regions computed from data-based estimates of $\mathcal{G}$. See text and Fig. 1 for definition of regions. The deep ocean is defined as depths below 1500 m.

Region	Global	Deep ocean (>1500 m)	0–500 m	500–1500 m	1500–3000 m	>3000 m
NA	26.0 ± 1.5	33.0 ± 2	6.0 ± 0.5	17.0 ± 1.2	30.5 ± 3.1	36.5 ± 3.5
ANT	39.0 ± 2.5	48.0 ± 3.2	9.5 ± 1	29.5 ± 2.6	45.0 ± 3.7	53.0 ± 4.7
SUBANT	18.0 ± 1	13.0 ± 1.1	23.0 ± 2	29.0 ± 3.1	17.0 ± 1.6	7.5 ± 1.8
TROP	4.5 ± 0.5	0.5 ± 0.1	27.5 ± 2.5	3.0 ± 0.5	0.7 ± 0.1	0.2 ± 0.1
STROP	8.1 ± 0.6	2.5 ± 0.2	29.0 ± 3	14.5 ± 2	3.2 ± 0.4	0.9 ± 0.2
NPAC	4.0 ± 0.3	3.0 ± 0.2	6.0 ± 0.5	7.0 ± 1	3.6 ± 0.5	1.8 ± 0.5

Table 2
Atlantic basin volumetric source fractions (%) for different surface regions computed from data-based estimates of $\mathcal{G}$. See text and Fig. 1 for definition of regions. The deep ocean is defined as depths below 1500 m.

Source region	Full depth	Deep ocean (>1500 m)	0–500 m	500–1500 m	1500–3000 m	>3000 m
NA	53.6 ± 4.5	66.9 ± 6	14.1 ± 1.5	33.8 ± 2.5	63.0 ± 5.5	72.5 ± 6.1
ANT	21.0 ± 2	21.5 ± 2	14.0 ± 1.5	25.1 ± 3	21.0 ± 2.8	22.5 ± 3.1
SUBANT	11.6 ± 0.9	7.4 ± 0.8	16.8 ± 2	20.6 ± 2	10.3 ± 1.5	3.4 ± 0.5
TROP	2.8 ± 0.4	0.4 ± 0.1	17.4 ± 2	1.2 ± 0.2	0.5 ± 0.1	0.2 ± 0.1
STROP	10.6 ± 1	3.3 ± 0.5	37.5 ± 3.4	18.9 ± 2	4.7 ± 0.6	0.7 ± 0.1
NPAC	0.4 ± 0.1	0.5 ± 0.2	0.0	0.4 ± 0.1	0.3 ± 0.1	0.6 ± 0.2

Table 3
Pacific basin volumetric source fractions (%) for different surface regions computed from data-based estimates of $\mathcal{G}$. See text and Fig. 1 for definition of regions. The deep ocean is defined as depths below 1500 m.

Source region	Full depth	Deep ocean (>1500 m)	0–500 m	500–1500 m	1500–3000 m	>3000 m
NA	16.2 ± 1.5	20.9 ± 2	3.2 ± 0.5	10.9 ± 1	18.1 ± 2	24.5 ± 3
ANT	42.5 ± 3	54.4 ± 4	4.2 ± 0.6	28.3 ± 2.8	50.3 ± 4.5	60.9 ± 6.5
SUBANT	21.3 ± 2	16.7 ± 1.5	22.5 ± 2.5	31.7 ± 3	21.5 ± 2.5	10.4 ± 1.5
TROP	5.6 ± 0.8	0.6 ± 0.1	33.3 ± 3.5	4.0 ± 0.6	0.9 ± 0.2	0.3 ± 0.1
STROP	7.4 ± 1	2.5 ± 0.3	26.0 ± 3	12.7 ± 1.5	2.9 ± 0.5	1.2 ± 0.4
NPAC	6.9 ± 0.8	4.9 ± 0.5	10.8 ± 0.9	12.3 ± 1.3	6.1 ± 0.7	2.7 ± 0.3

3.2. The ideal mean age of the ocean

We now consider the temporal information of the boundary propagator. Tracers such as CFCs and ^{14}C have long been used to estimate the "age" of water. However, as noted, interpretation of tracer-derived ages poses certain challenges, since in the presence of mixing there is no unique time scale for transport of fluid from the mixed layer into the interior. Instead, analyses of tracer data (e.g. Hall et al., 2004) suggests strong mixing, and hence a broad range of time scales. This is quantitatively captured by the boundary propagator. We first discuss the transit-time distribution (TTD) $\bar{\mathcal{G}}(\mathbf{x},\xi)\equiv\sum_i \mathcal{G}(\mathbf{x}|\xi,i)$, which is the distribution of times since contact anywhere with the global sea surface.

Fig. 3 shows our inverse estimate of $\mathcal{G}$as a function of transit time at a depth of 600 m, 1500 m, and 2950 m at several select locations (see inset map) along the path of the "conveyor belt" circulation, starting in the North Atlantic and ending in the North Pacific. The transit time at which the TTDs peak, what might be called the "modal age", shifts toward older values along the path of the "conveyor", while the peak value decreases, as might be expected from a signal that attenuates downstream of its source. The TTDs are also quite broad, in agreement with previous observational (Hall et al., 2004; Waugh et al., 2004) and model studies (Khatiwala et al., 2001; Maltrud et al., 2009; Peacock and Maltrud, 2006; Primeau, 2005). A number of the TTDs at 1500 m also exhibit a multimodal structure indicating significant contributions from more than one source region (SO, SUBANT, and NPAC in this case).

Another notable feature of the TTDs is their long tail, which has a considerable impact on the *average* length of time water has been isolated from the atmosphere. This quantity, known as the ideal mean age, Γ, is defined as the first moment of $\bar{\mathcal{G}}$:

$$\Gamma(\mathbf{x}) = \int_0^\infty d\xi\,\xi\,\bar{\mathcal{G}}(\mathbf{x},\xi). \tag{3}$$

Fig. 4 shows the mean age distribution of the ocean averaged over depths greater than 1500 m. The pattern is a familiar one, with relatively young waters in the North Atlantic and Southern Ocean. The oldest waters, with ages between 1300 and 1400 y, are found in the North Pacific. This is somewhat younger than mean ages simulated in ocean general circulation models (England, 1995; Peacock and Maltrud, 2006; Primeau, 2005). Peacock and Maltrud (2006), for example, found ages of ~1700 y in the North Pacific. But we note that simulated ages tend to be sensitive to both resolution and parameterization of mixing processes (England, 1995; Peacock and Maltrud, 2006). Furthermore, because of the entropic error (see HPSK10), our estimates are also subject to considerable uncertainty, in places as high as several hundred years. However, when averaged over large regions, the errors are significantly smaller, and our estimate of ≈1350 y for the mean age of the deep Pacific is robust. This value is also consistent with the value of 1300 (−50/+200) y obtained by Holzer and Primeau (2010) for two profiles in the North Pacific using a similar approach, but with an additional constraint provided by ^{39}Ar data.

4. Implications for radiocarbon-based estimates of "age"

It is instructive to compare our estimate of the ideal mean age with previous computations of "age" based on radiocarbon. Radiocarbon, and other transient tracer-derived, ages have been widely used in ocean and climate research as a measure of signal propagation or "turnover" time. Indeed, much of our current knowledge regarding the ventilation of the deep ocean, both present and past, is based on ^{14}C. Radiocarbon is produced in the atmosphere and enters the ocean through air–sea gas exchange. The "conventional" ^{14}C age is computed on the assumption that surface waters are in equilibrium with the atmosphere and thus have an age of zero. However, the assumption of equilibration with the atmosphere is known to be incorrect. The time scale for isotopic equilibration between the surface ocean and the atmosphere is ~10 y (Broecker and Peng, 1982), and the conventional ^{14}C age of surface waters, known as the "reservoir age", can be several hundred years. It also varies significantly from one region to another (Broecker et al., 1985; Butzin et al., 2005), as is evident in Fig. 5 based on data from the GLODAP database (Key et al., 2004). As demonstrated in a numerical model by Campin et al. (1999), the uncertainty in the reservoir age poses a fundamental problem for interpreting radiocarbon data.

Recognizing this, Matsumoto (2007) attempted to account for the spatial variability by assuming two end-member mixing between a "northern" and a "southern" source with specified ^{14}C concentrations computed by Broecker et al. (1998) using PO_4^*. Fig. 6 compares their resulting age estimate (right) (called "circulation" age by Matsumoto) with the conventional ^{14}C age (left) based on the GLODAP data (Key et

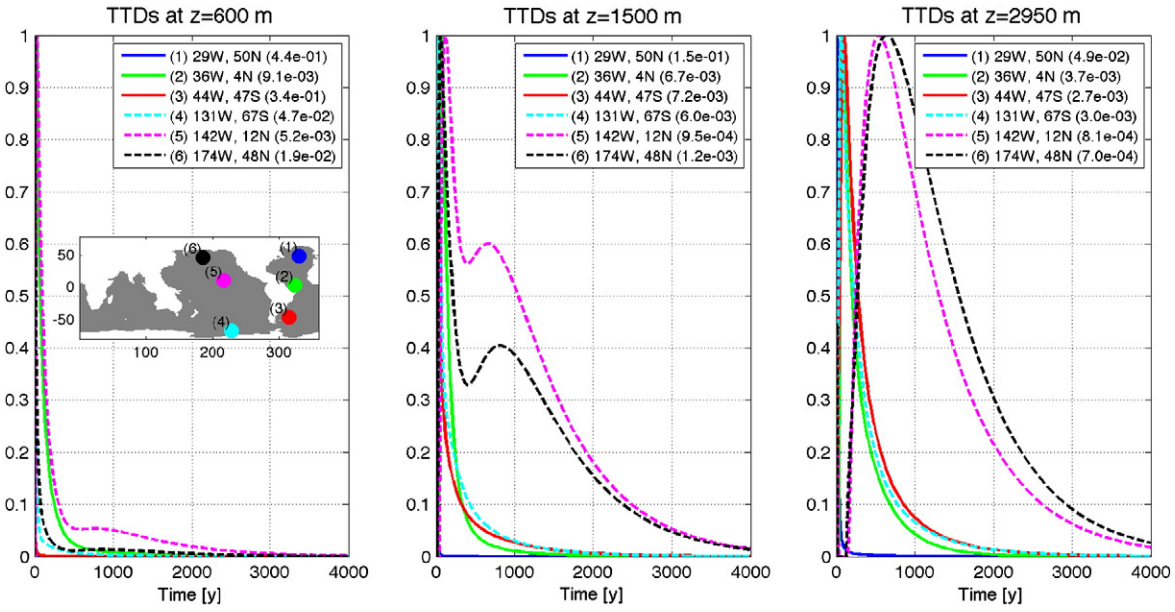

Fig. 3. Transit-time distributions at selected locations at (from left to right) 600 m, 1500 m, and 2950 m. See the inset map in the first panel for locations. Note that the TTDs have been scaled by their maximum value at each location (number in brackets in legend).

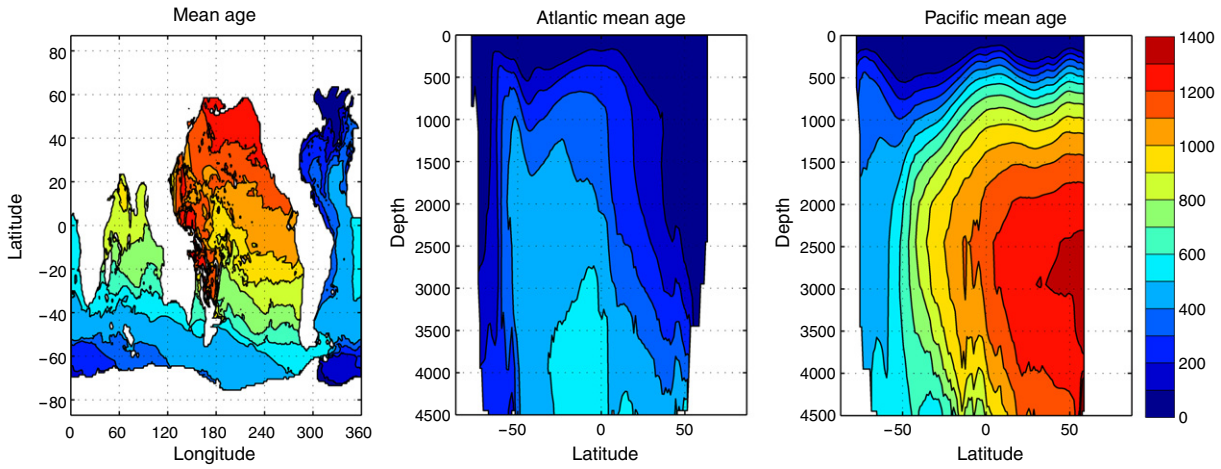

Fig. 4. Mean age distribution of the ocean. Left to right: Depth-weighted average from 1500 m to bottom; Atlantic zonal average; and Pacific zonal average.

al., 2004). Conventional ^{14}C ages are much higher than circulation ages. In the North Pacific, the former are well over 2000 y, while the latter are $\approx$600–800 y. Our estimate of the ideal mean age (Fig. 4) is intermediate between the two. Matsumoto (2007) assesses the error in the circulation age at $\pm$75 y, but did not consider errors associated with the mapping of the sparsely sampled data, or the uncertainty in estimating source fractions and their corresponding ^{14}C values.

While an improvement, it is unlikely that a two end-member description of the deep ocean can adequately account for the spatial variability in the surface radiocarbon (Fig. 5) (e.g., Campin et al., 1999). Furthermore, the long time scales for transport into the deep ocean coupled with the exponential decay of radiocarbon introduce the possibility of ^{14}C ages being biased toward younger values, a notion sometimes known as "nonlinear mixing" (e.g., Deleersnijder et al., 2001; Khatiwala et al., 2001).

To quantify the impact of these effects, Holzer et al. (2010) have recently applied the boundary propagator approach to analyze the difference between the radiocarbon age, Γ_C, and the mean age, Γ. Following them, we define Γ_C via:

$$^{14}C(\mathbf{x}) = {}^{14}C_o(\mathbf{x})e^{-\lambda\Gamma_C(\mathbf{x})}, \tag{4}$$

where, λ is the radioactive decay constant, and the "initial" concentration, $^{14}C_o$, is a fraction-weighted average of the surface concentration $^{14}C^s$:

$$^{14}C_o(\mathbf{x}) = \sum_i f_i(\mathbf{x})\,{}^{14}C_i^s. \tag{5}$$

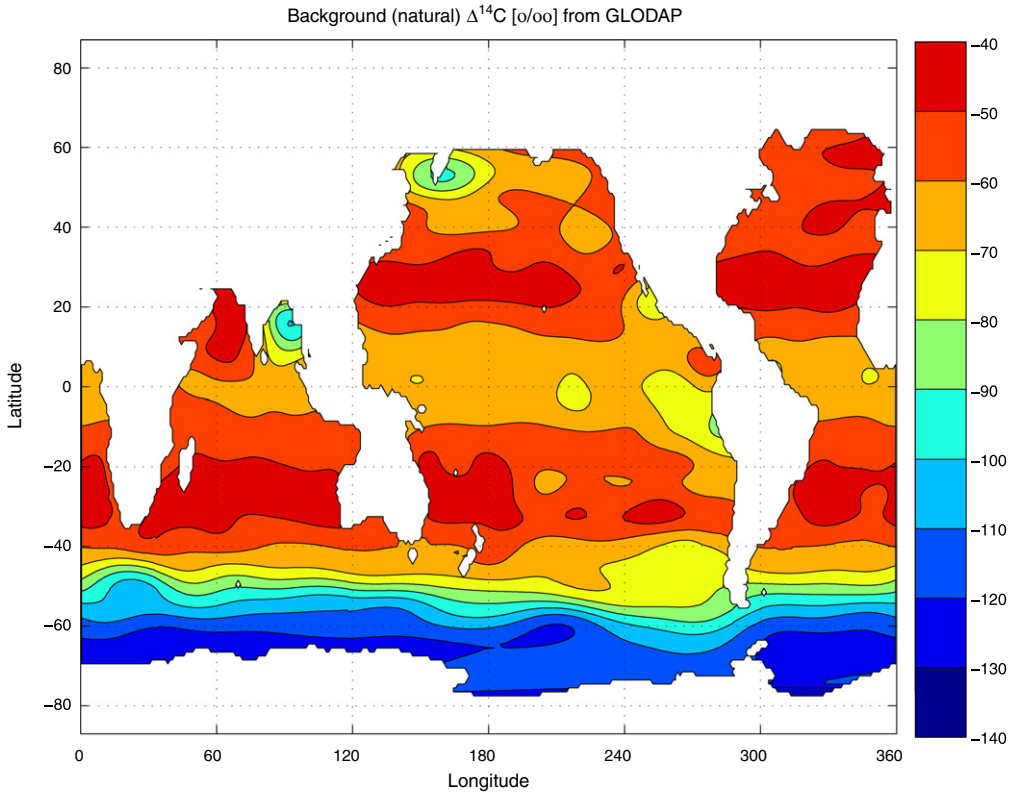

Fig. 5. Surface distribution of natural radiocarbon from the GLODAP database.

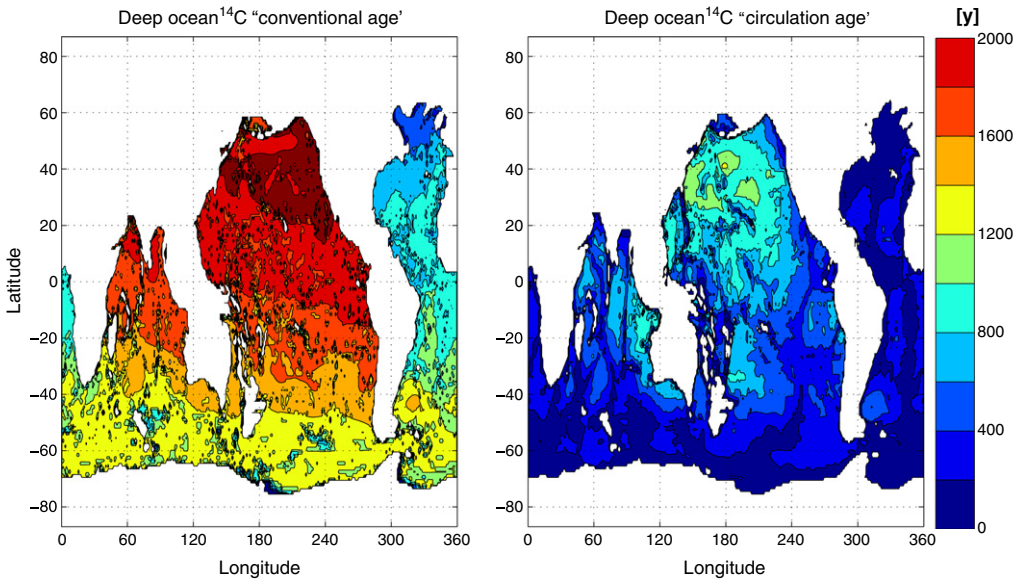

Fig. 6. Depth-averaged (1500 m to bottom) radiocarbon age. Left: Conventional radiocarbon age computed as $-8033\ln(1+\Delta^{14}C/1000)$, where $\Delta^{14}C$ is the background radiocarbon estimate from GLODAP (Key et al., 2004); right: "Circulation" age computed by Matsumoto (2007).

Combining our estimates of f_i with the surface natural ^{14}C field from GLODAP (Fig. 5), we have computed the "initial" radiocarbon in the deep ocean. The result is displayed in Fig. 7, expressed as an equivalent reservoir age: $-\lambda^{-1}ln(^{14}C_o/^{14}C_{eq})$, where $^{14}C_{eq}$ is the concentration in equilibrium with the atmosphere. The figure shows that spatial variability in the surface ^{14}C translates into variability in the "initial" radiocarbon concentration and reservoir age. Note, in particular, the high values around Antarctica. Upwelling of "old" waters depleted in radiocarbon, combined with a finite time scale for reaching equilibrium with the atmosphere (e.g., Broecker et al., 1985), leads to the low $\Delta^{14}C$ values seen in surface waters around the Antarctic margin (Fig. 5).

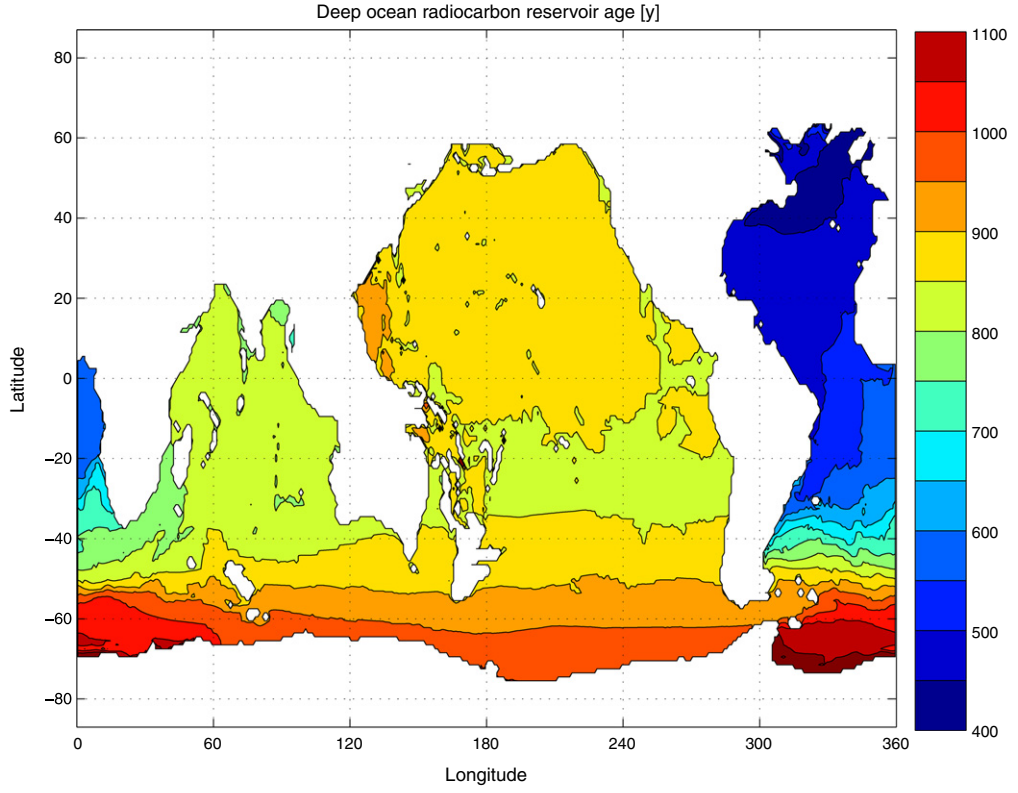

Fig. 7. Average reservoir age correction for waters below 1500 m.

Using the relationship between the f_i and $\mathcal{G}$'s (Eq. (2)), HPSK10 show that Eq. (4) for the ^{14}C concentration (and Γ_C) can, to a good approximation, be written in terms of Γas:

$$^{14}C(\mathbf{x}) = {}^{14}C_o(\mathbf{x})e^{-\lambda\Gamma(\mathbf{x})}\left[1-\lambda\sum_i \frac{\left({}^{14}C_i^s - \overline{{}^{14}C^s}\right)}{{}^{14}C_o(\mathbf{x})}\delta\Gamma_i(\mathbf{x}) + \lambda^2\Delta^2(\mathbf{x})\frac{\overline{{}^{14}C^s}}{{}^{14}C_o(\mathbf{x})} + \lambda^2\sum_i \frac{\left({}^{14}C_i^s - \overline{{}^{14}C^s}\right)}{{}^{14}C_o(\mathbf{x})} D_i^2(\mathbf{x}) + \cdots\right], \quad (6)$$

where the overlines are spatial averages over the sea surface,

$$\delta\Gamma_i(\mathbf{x}) \equiv \int_0^\infty d\xi(\xi - \Gamma(\mathbf{x}))\mathcal{G}(\mathbf{x}|\xi, i),$$

and,

$$D_i^2(\mathbf{x}) \equiv \frac{1}{2}\int_0^\infty d\xi(\xi-\Gamma(\mathbf{x}))^2\mathcal{G}(\mathbf{x}|\xi,i) \text{and } \Delta^2(\mathbf{x}) \equiv \sum_i D_i^2(\mathbf{x}).$$

Comparing Eqs. (4) and (6) we see that $\Gamma_C \approx \Gamma$ if the second and higher terms in Eq. (6) can be neglected. These terms arise from (1) spatial variations in the surface concentration, (2) variations $\delta\Gamma$ in the mean transit time from the different surface regions, and (3) the width Δ of the TTD relative to the decay time scale for radiocarbon ($1/\lambda \sim 8300$ y). Radiocarbon data show that the first and second of these is quite small. To illustrate the third, Fig. 8 shows the relative difference between the mean and radiocarbon ages for the 1-d advection–diffusion equation (which has a single "source" at the origin so that $\delta\Gamma = 0$) as a function of Γ and the ratio Δ/Γ. Also displayed (white dots) are our estimates of Γ and Δ/Γ for the deep ocean derived from the BPs. While the two are not quite comparable, it does suggest that the ocean lies in a region of parameter space where the impact of finite BP width is quite small. Thus, if the "initial" radiocarbon distribution can be well estimated, we should expect good agreement between the ideal mean age and the radiocarbon age computed from Eq. (4). Consistent with this, we find that differences between the ideal mean ages and the radiocarbon ages are generally less than 50 y (Fig. 9) implying that nonlinear mixing has a negligible impact on ^{14}C age. This result is in accord with the explicit numerical simulations of Deleersnijder et al. (2001) showing a difference on the order of 5% (see also Hall et al. (2002) and Delhez et al. (2003)).

5. Summary and conclusions

To summarize, we have presented the first data-based estimate of the joint distribution of the age and surface origin of ocean waters. This distribution, which is also a boundary propagator Green function, rigorously quantifies ventilation accounting for the multiplicity of transport pathways and transit times that characterizes ocean circulation. Our results show that roughly 80% of the deep ocean below 1500 m is ventilated from the high latitude Southern Ocean and North Atlantic. While broadly consistent with the widely held view of the deep ocean as a mixture of "northern" and "southern" source waters (Broecker et al., 1998), in contrast to previous work we find that these two sources contribute unequally, with the Southern Ocean dominating.

We find that the ideal mean age of the deep North Pacific is 1360 $\pm$350 y. This value is considerably younger than the corresponding conventional radiocarbon age, which is computed on the assumption that surface waters are in equilibrium with the atmosphere and thus have an age of zero. To account for the known disequilibrium between the atmosphere and surface waters, conventional ^{14}C ages are typically corrected for the reservoir age, i.e., the conventional ^{14}C age of surface waters. This correction, which can be several hundred years, is however spatially highly variable, leading to significant uncertainty in interpreting radiocarbon data (Campin et al., 1999). To reconcile our estimate of the ideal mean age with ventilation age estimates based on radiocarbon, we used the estimated boundary propagator to construct a water mass fraction-weighted surface "initial" radiocarbon concentration that can serve as an accurate reservoir age.

While the need for a reservoir age correction has long been appreciated (Broecker and Peng, 1982), to our knowledge this is the first global, observationally-based, spatially-distributed estimate of this quantity

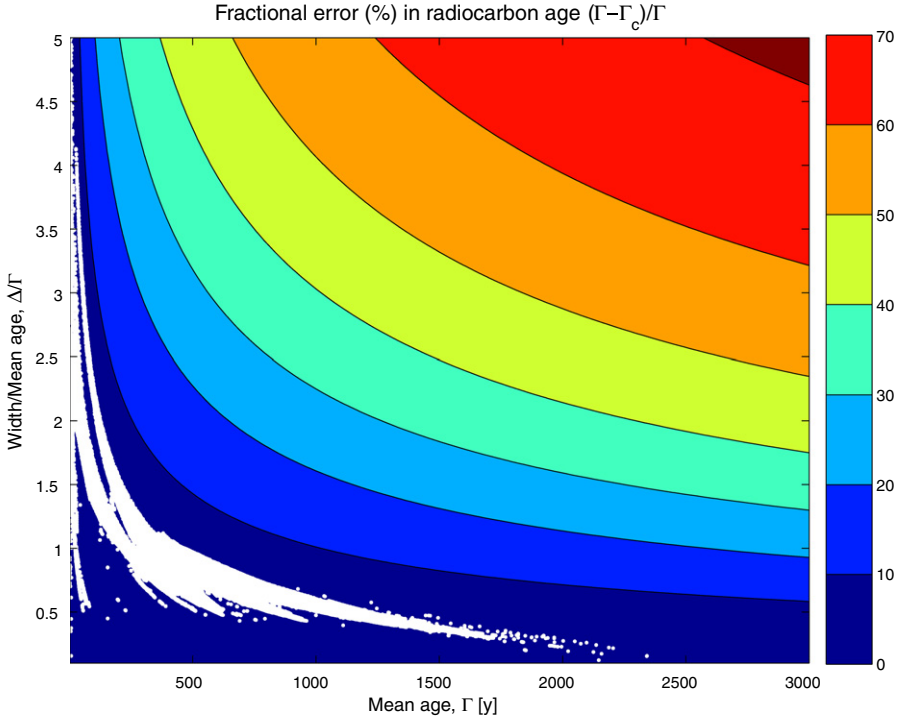

Fig. 8. Fractional difference between the mean and radiocarbon ages as a function of Γ and Δ/Γ for the 1-d advection–diffusion (contours). The white dots are (Γ,Δ/Γ) for the deep ocean derived from estimates of the BP.

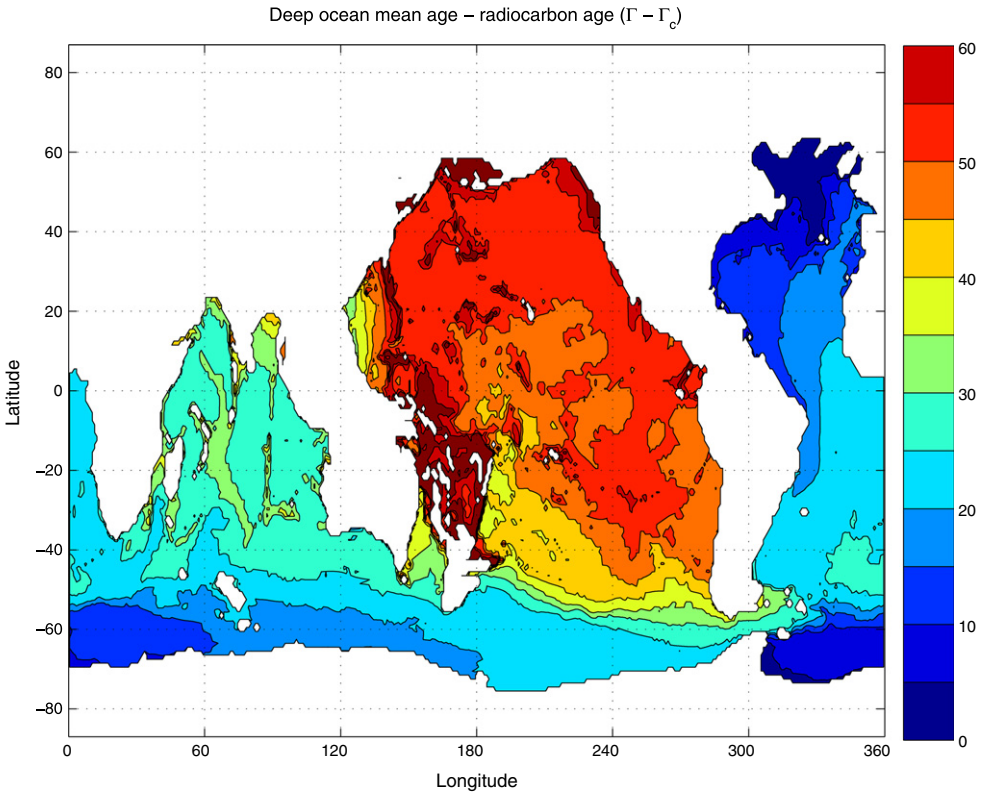

Fig. 9. Depth-average (1500 m to bottom) of difference between mean age and radiocarbon age.

that can be applied to radiocarbon data. Existing observational estimates (e.g., http://radiocarbon.ldeo.columbia.edu/research/resage.htm and http://calib.qub.ac.uk/marine/) are at a sparse number of discrete locations typically along the continental margin, while global estimates are based on ocean models (e.g., Butzin et al., 2005). Radiocarbon ages corrected for this initial reservoir age are found to be in good agreement (within 5%) with our ideal age estimate, demonstrating the necessity of taking into account the spatially variable surface radiocarbon field when computing ventilation ages using radiocarbon. Furthermore, in line with previous numerical simulations (e.g., Deleersnijder et al., 2001), our results also imply that the finite width of the transit-time distribution leads to only a weak nonlinear mixing effect on ^{14}C ages.

We note that our results are subject to the caveat that we assume a steady state ocean circulation, an assumption dictated by the difficulty in constraining temporal variability in circulation rather than because of any fundamental limitation of the Green function formalism or inverse methodology. While this may introduce quantitative errors in our various estimates, we expect that the broad conclusions presented above to be fairly robust. In particular, the analysis of radiocarbon ages presented above (Eq. (6)) should hold even in the time-dependent case when $^{14}C_o$, Γ_C, and Γ become functions of time.

Temporal variability in $^{14}C_o$, and hence Γ_C (Eq. (4)), can also be introduced if ocean circulation is in steady state but the atmospheric radiocarbon is not constant. In that case, the broadness of the TTD will have a significant impact on the mean age inferred from radiocarbon if atmospheric radiocarbon is changing sufficiently rapidly as is the case for the current atmosphere which is still adjusting to the recent bomb pulse and, as shown by the IntCal09 reconstructions (Reimer et al., 2009), for much of the paleo record. (According to the IntCal09 record, atmospheric radiocarbon activity has been relatively constant over the last few millennia.) Recently, DeVries and Primeau (2010) have attempted to take into account the broadness of the TTD and the changing atmospheric radiocarbon levels implied by the IntCal09 reconstruction for the interpretation of a sediment core from the North Pacific. Our work suggests that when changes in atmospheric radiocarbon take place over periods of time comparable to the radioactive decay timescale of radiocarbon, the impact of diffusive mixing implied by the broadness of the TTD is negligible provided one can properly account for the mixing of end-members with different reservoir ages. Our work furthermore shows that very few places in the deep modern ocean can be viewed as being composed of only one source-water type as is assumed in most sediment core analyses. The development of a suite of paleoceanographic tracers capable of identifying the surface origin of deep ocean water masses should therefore be a priority if we are to interpret properly the ^{14}C record in sediments.

Acknowledgments

We thank K. Matsumoto for making available his “circulation age” estimates shown in Fig. 6. This work was supported by US NSF grants OCE-1060804 (SK), OCE-0726871 (FP), and ATM-0854711 (MH). LDEO contribution number 7522.

References

Anderson, L.A., Sarmiento, J.L., 1995. Global ocean phosphate and oxygen simulations. Glob. Biogeochem. Cycles 9, 621–636.
Antonov, J.I., Locarnini, R.A., Boyer, T.P., Mishonov, A.V., Garcia, H.E., 2006. World Ocean Atlas 2005, volume 2: salinity. NOAA Atlas NESDIS 62. U.S. Government Printing Office, Washington, DC.
Broecker, W.S., 1991. The Great Conveyor Belt. Oceanography 4, 79–89.
Broecker, W.S., Peng, T.-H., 1982. Tracers in the Sea. Lamont–Doherty Earth Obs.
Broecker, W.S., Peng, T.H., Ostlund, G., Stuiver, M., 1985. The distribution of bomb radiocarbon in the ocean. J. Geophys. Res. 90, 6953–6970.
Broecker, W.S., Peacock, S.L., Walker, S., Weiss, R., Fahrbach, E., Schroeder, M., Mikolajewicz, U., Heinze, C., Key, R.M., Peng, T., Rubin, S., 1998. How much deep water is formed in the southern ocean. J. Geophys. Res. 103, 15833–15844.
Butzin, M., Prange, M., Lohmann, G., 2005. Radiocarbon simulations for the glacial ocean: the effects of wind stress, Southern Ocean sea ice and Heinrich events. Earth Planet. Sci. Lett. 235, 45–61.
Campin, J., Fichefet, T., Duplessy, J., 1999. Problems with using radiocarbon to infer ocean ventilation rates for past and present climates. Earth Planet. Sci. Lett. 165, 17–24.
De Brauwere, A., Jacquet, S.H.M., De Ridder, F., Dehairs, F., Pintelon, R., Schoukens, J., Baeyens, W., 2007. Water mass distributions in the Southern Ocean derived from

a parametric analysis of mixing water masses. J. Geophys. Res. 112. doi:10.1029/2006JC003742.
Deleersnijder, E., Campin, J., Delhez, E., 2001. The concept of age in marine modelling: I. Theory and preliminary model results. J. Mar. Syst. 28, 229–267.
Delhez, E., Deleersnijder, E., Mouchet, A., Beckers, J., 2003. A note on the age of radioactive tracers. J. Mar. Syst. 38, 277–286.
DeVries, T., Primeau, F., 2010. An improved method for estimating water-mass ventilation age from radiocarbon measurements. Earth Planet. Sci. Lett. 295, 367–378.
DeVries, T., Primeau, F., 2011. Dynamically and observationally constrained estimates of water-mass distributions and ages in the global ocean. J. Phys. Oceanogr. 41, 2381–2401. doi:http://dx.doi.org/10.1175/JPO-D-10-05011.1.
England, M.H., 1995. The age of water and ventilation timescales in a global ocean model. J. Phys. Oceanogr. 25, 2756–2777.
Garcia, H.E., Locarnini, R.A., Boyer, T.P., Antonov, J.I., 2006a. World Ocean Atlas 2005, volume 3: dissolved oxygen, apparent oxygen utilization, and oxygen saturation. NOAA Atlas NESDIS 63. U.S. Government Printing Office, Washington, DC.
Garcia, H.E., Locarnini, R.A., Boyer, T.P., Antonov, J.I., 2006b. World Ocean Atlas 2005, volume 4: nutrients (phosphate, nitrate, silicate). NOAA Atlas NESDIS 64. U.S. Government Printing Office, Washington, DC.
Gebbie, G., Huybers, P., 2010. Total matrix intercomparison: a method for determining the geometry of water-mass pathways. J. Phys. Oceanogr. 40. doi:10.1175/2010JPO4272.1.
Haine, T.W.N., Richards, K.J., 1995. The influence of the seasonal mixed layer on oceanic uptake of CFCs. J. Geophys. Res. 100, 10727–10744.
Hall, T.M., Haine, T.W.N., Waugh, D.W., 2002. Inferring the concentration of anthropogenic carbon in the ocean from tracers. Glob. Biogeochem. Cycles 16. doi:10.1029/2001GB001835.
Hall, T.M., Waugh, D.W., Haine, T.W.N., Robbins, P.E., Khatiwala, S., 2004. Estimates of anthropogenic carbon in the Indian Ocean with allowance for mixing and time-varying air-sea CO_2 disequilibrium. Glob. Biogeochem. Cycles 18. doi:10.1029/2003GB002120.
Holzer, M., Hall, T.M., 2000. Transit-time and tracer-age distributions in geophysical flows. J. Atmos. Sci. 57, 3539–3558.
Holzer, M., Primeau, F., 2006. The diffusive ocean conveyor. Geophys. Res. Lett. 33. doi:10.1029/2006GL026232.
Holzer, M., Primeau, F., 2008. The path-density distribution of oceanic surface-to-surface transport. J. Geophys. Res. 113. doi:10.1029/2006JC003976.
Holzer, M., Primeau, F., 2010. Improved constraints on transit time distributions from argon 39: a maximum entropy approach. J. Geophys. Res. 115. doi:10.1029/2010JC006410.
Holzer, M., Primeau, F., Smethie, W., Khatiwala, S., 2010. Where and how long ago was water in the western North Atlantic ventilated? Maximum-entropy inversions of bottle data from WOCE line A20. J. Geophys. Res. 115. doi:10.1029/2009JC005750.
Johnson, G.C., 2008. Quantifying Antarctic bottom water and North Atlantic deep water volumes. J. Geophys. Res. 113. doi:10.1029/2007JC004477.
Key, R.M., Kozyr, A., Sabine, C., Lee, K., Wanninkhof, R., Bullister, J., Feely, R.A., Millero, F., Mordy, C., Peng, T.-H., 2004. A global ocean carbon climatology: results from GLODAP. Glob. Biogeochem. Cycles 18. doi:10.1029/2004GB002247.
Khatiwala, S., Visbeck, M., Schlosser, P., 2001. Age tracers in an ocean GCM. Deep-Sea Res. I 48, 1423–1441.
Khatiwala, S., Primeau, F., Hall, T., 2009. Reconstruction of the history of anthropogenic CO_2 concentrations in the ocean. Nature 462. doi:10.1038/nature08526.
Locarnini, R.A., Mishonov, A.V., Antonov, J.I., Boyer, T.P., Garcia, H.E., 2006. World Ocean Atlas 2005, Volume 1: temperature. NOAA Atlas NESDIS 61. U.S. Government Printing Office, Washington, DC.
Maltrud, M., Bryan, F., Peacock, S., 2009. Boundary impulse response functions in a century-long eddying global ocean simulation. Environ. Fluid Mech.. doi:10.1007/s10652-009-9154-3
Matsumoto, K., 2007. Radiocarbon-based circulation age of the world oceans. J. Geophys. Res. 112. doi:10.1029/2007JC004095.
Memery, L., Wunsch, C., 1990. Constraining the North Atlantic circulation with tritium data. J. Geophys. Res. 95, 5229–5256.
Peacock, S., Maltrud, M., 2006. Transit-time distributions in a global ocean model. J. Phys. Oceanogr. 36, 474–495.
Primeau, F., 2005. Characterizing transport between the surface mixed layer and the ocean interior with a forward and adjoint global ocean transport model. J. Phys. Oceanogr. 35, 545–564.
Reimer, P.J., Baillie, M.G.L., Bard, E., Bayliss, A., Beck, J.W., Blackwell, P.G., Bronk Ramsey, C., Buck, C.E., Burr, G.S., Edwards, R.L., Friedrich, M., Grootes, P.M., Guilderson, T.P., Hajdas, I., Heaton, T.J., Hogg, A.G., Hughen, K.A., Kaiser, K.F., Kromer, B., McCormac, F.G., Manning, S.W., Reimer, R.W., Richards, D.A., Southon, J.R., Talamo, S., Turney, C.S.M., van der Plicht, J., Weyhenmeyer, C.E., 2009. IntCal09 and Marine09 radiocarbon age calibration curves, 0–50,000 years cal BP. Radiocarbon 51 (4), 1111–1150.
Schlitzer, R., 1993. Determining the mean, large-scale circulation of the Atlantic with the adjoint method. J. Phys. Oceanogr. 23, 1935–1952.
Stammer, D., Ueyoshi, K., Köhl, A., Large, W.G., Josey, S.A., Wunsch, C., 2004. Estimating air-sea fluxes of heat, freshwater, and momentum through global ocean data assimilation. J. Geophys. Res. 109. doi:10.1029/2003JC002082.
Stommel, H., 1979. Determination of water mass properties of water pumped down from the Ekman layer to the geostrophic flow below. Proc. Natl. Acad. Sci. 76, 3051–3055.
Tarantola, A., 2005. Inverse problem theory and methods for model parameter estimation. Soc. Ind. Appl. Math. 342 pages/Softcover/ISBN-13: 978-0-898715-72-9/ISBN-10: 0-89871-572-5/.
Tomczak, M., 1981. Bass Strait water intrusions in the Tasman Sea and mean temperature–salinity curves. Aust. J. Mar. Freshw. Res. 32, 699–708.
Tomczak, M., Large, D.G.B., 1989. Optimum multiparameter analysis of mixing in the thermocline of the eastern Indian Ocean. J. Geophys. Res. 94. doi:10.1029/JC094iC11p16141.
Waugh, D.W., Haine, T.W., Hall, T.M., 2004. Transport times and anthropogenic carbon in the subpolar North Atlantic Ocean. Deep Sea Res. I 51, 1475–1491.
Williams, R.G., Marshall, J.C., Spall, M.A., 1995. Does Stommel's mixed layer demon work? J. Phys. Oceanogr. 25, 3089–3102.
Wunsch, C., 1984. An eclectic Atlantic Ocean circulation model. Part I: the meridional flux of heat. J. Phys. Oceanogr. 14, 1712–1733.
Wunsch, C., Heimbach, P., 2007. Practical global oceanic state estimation. Physica D 230, 197–208.
Wunsch, C., Heimbach, P., 2008. How long to oceanic tracer and proxy equilibrium? Quat. Sci. Rev. 27, 637–651.